Noushin Torabian,[1] Véronique Favier,[2] Saeed Ziaei-Rad,[3]
Justin Dirrenberger,[2] Frédéric Adamski,[2] and Nicolas Ranc[2]

Calorimetric Studies and Self-Heating Measurements for a Dual-Phase Steel Under Ultrasonic Fatigue Loading

Citation

Torabian, N., Favier, V., Ziaei-Rad, S., Dirrenberger, J., Adamski, F., and Ranc, N., "Calorimetric Studies and Self-Heating Measurements for a Dual-Phase Steel Under Ultrasonic Fatigue Loading," *Fatigue and Fracture Test Planning, Test Data Acquisitions and Analysis*, *ASTM STP1598*, Z. Wei, K. Nikbin, P. C. McKeighan, and D. G. Harlow, Eds., ASTM International, West Conshohocken, PA, 2017, pp. 81–93, http://dx.doi.org/10.1520/STP159820160053[4]

ABSTRACT

The objective of the present research is to study the self-heating behavior of a dual-phase (DP) steel under ultrasonic fatigue loading and to investigate the effect of frequency on intrinsic heat dissipation of the material. The steel studied in this work is DP600 commercial DP steel. Fatigue tests were conducted using an ultrasonic fatigue machine at a testing frequency of 20 kHz with flat specimens. An infrared camera was used to measure the mean temperature evolution during the tests. A specific form of heat diffusion equation was adopted in this work to calculate the heat dissipation per cycle from temperature measurements. The variation of this dissipation versus stress amplitude in cyclic loading was also studied.

Keywords
ultrasonic fatigue, infrared thermography, dual-phase steel

Introduction

Since the first relevant conference in Paris in 1998 [1], the fatigue behavior of metallic materials in the very high cycle fatigue (VHCF) regime ($N_f \geq 10^7$) has been investigated by various research groups. Ultrasonic fatigue testing [2,3] is an effective tool to carry out VHCF tests. Due to the extremely high loading frequency of 20 kHz, an ultrasonic fatigue machine considerably reduces the testing time and makes it possible to investigate the VHCF properties of different high-strength steels in a reasonable time. For instance, it takes 14 h to reach 10^9 cycles with ultrasonic loading, while using a conventional fatigue machine with a working frequency of 100 Hz, a time period of four months is required to go up to 10^9 cycles. With regard to the application of the ultrasonic testing frequency, most researchers believe that frequency effect itself is small in most cases at low stress amplitudes and does not change the essence of fatigue [4–6]. However, the frequency effect is not clear for all metallic materials such as ferritic-martensitic dual-phase (DP) steels. Moreover, the thermal effect induced by loading with ultrasonic frequency is still questionable. The aim of the present work is to conduct a thermography study on a DP steel under ultrasonic fatigue loading at low stress amplitudes.

DP steels are a group of advanced steels that contain hard martensite islands dispersed in a soft ferrite matrix. Due to its characteristics of high strength, good ductility, and high initial work hardening rates, DP steel has a broad application in the automotive industry.

In several research works, the dissipated energy was deduced from self-heating measurements of DP steels during low-frequency fatigue loadings [7–11]. With respect to ultrasonic fatigue testing (20 kHz), Blanche et al. [12] as well as Ranc et al. [13] developed methods to identify dissipative fields from infrared (IR) thermography measurements. The method developed by Blanche et al. [14] was also applied to compare the dissipative response during cycling of three single-phase metals: copper, alpha-brass, and alpha-iron.

The present paper studies the thermal response of DP600 commercial steel under ultrasonic fatigue loading. Successive fatigue tests with increasing stress amplitude are carried out by means of an ultrasonic fatigue machine with the working frequency of 20 kHz. IR thermography is used to record the mean temperature on the surface of the specimen. Self-heating diagrams are developed for this material based on mean temperature. The mean dissipated energy per cycle is estimated as a function of the stress amplitude.

Material and Experimental Procedure

MATERIAL CHARACTERIZATION

The material used in this study is DP600 steel that was received as sheets 3 mm thick. This commercial ferritic-martensitic DP steel contains 15 wt % martensite. **Fig. 1** shows

FIG. 1 SEM micrograph of the DP600 sample. (Bright grains are martensite and dark grains are ferrite.)

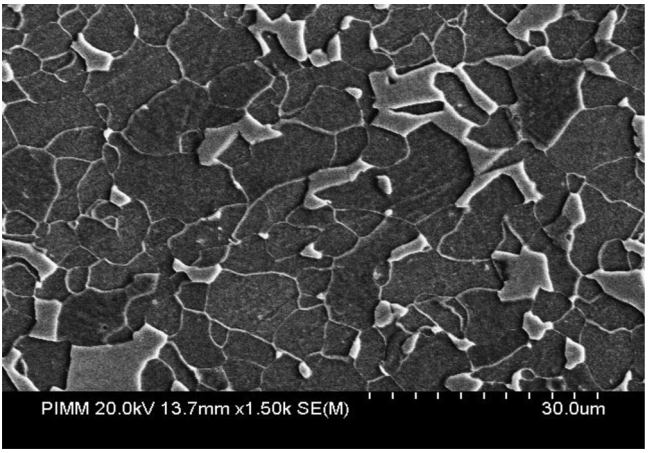

the microstructure of the material obtained from scanning electron microscope (SEM) observations. Table 1 presents the chemical composition of the material. The mechanical properties of DP600 in the transverse direction are presented in Table 2.

ULTRASONIC FATIGUE LOADINGS

Fatigue tests are conducted with flat specimens using an ultrasonic fatigue machine at a testing frequency of 20 kHz and by applying a sinusoidal displacement wave. The specimen dimensions are calculated so that the free resonant frequency of the specimen in the first longitudinal mode is 20 kHz. The specimens are machined in the transverse direction. All specimens are mechanically and then electrolytically polished to remove all hardened layers on the specimen surface and, consequently, to release the residual stresses. Fig. 2 illustrates the geometry of the fatigue specimens.

In all of the tests, the loading ratio is $R = -1$. During the tests, an IR camera with a spatial resolution of 0.024 mm per pixel is used to monitor the temperature field on the specimen surface. The acquisition frequency of the camera is 10 Hz. The specimen surface is painted in matte black to have a uniform surface emissivity close to 1. From the temperature measurements, the intrinsic dissipation is

TABLE 1 DP600 chemical composition [15].

Alloying Element	Mn	P	Si	Cr	C	S	Nb
% weight	0.93	0.04	0.213	0.727	0.0748	0.001	0.0425

TABLE 2 Mechanical properties of DP600 steel [15].

Young Modulus, GPa	Yield Strength, MPa	Ultimate Tensile Strength, MPa	Elongation, %
210	420	610	20

determined using a heat diffusion model as explained in the following section. Fig. 3 shows the ultrasonic equipment and the camera.

Successive steps of fatigue tests are conducted by increasing the stress amplitude from 57 MPa to 241 MPa, as shown schematically in Fig. 4. The tests are limited to low stress amplitudes (i.e., the stress values below the conventional fatigue limit, which equals 250 MPa) [15]. At each stress amplitude, the fatigue test is carried out up to 10^7 cycles, and the mean temperature evolutions are registered during the tests. At the end of each step, the testing machine is stopped and temperature measurements are continued for 2 min to record the cooling of the specimen after unloading. Between the two steps that follow, there is a time gap of around 10 min to restart at equilibrium. In all cases, the temperature is measured at the center of the gage part of the specimen.

DETERMINATION OF THE DISSIPATED ENERGY

In this study, the specific form of heat diffusion equation proposed by Boulanger et al. [7] is adopted to calculate the intrinsic dissipation from temperature measurements. Assuming there is no coupling between microstructure and temperature, and neglecting the convective terms, the heat diffusion equation (Eq 1) is written:

$$\rho C\dot{T} - div\left(k\,\overline{grad(T)}\right) = s_{the} + d_1 + r \tag{1}$$

where:

ρ = the mass density,

C = the specific heat,

FIG. 2 Fatigue test specimen geometry (all dimensions are in mm).

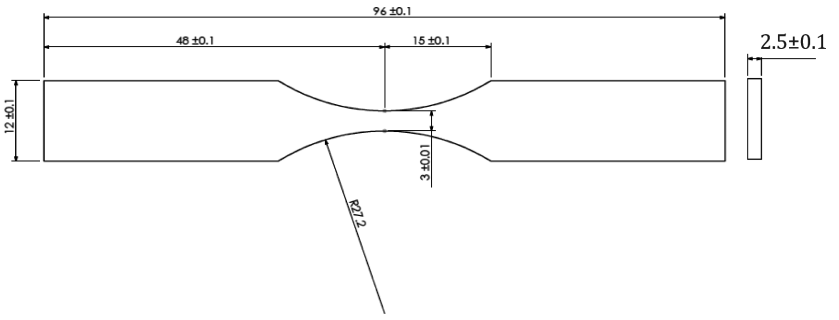

FIG. 3 Ultrasonic fatigue testing equipment.

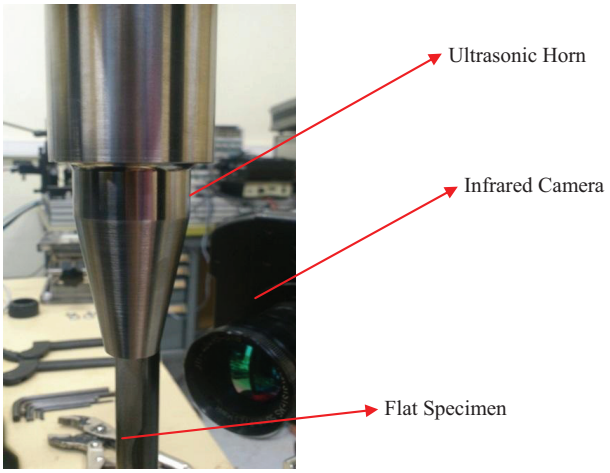

$\dot{T}$ = the time derivative of temperature,
k = the conduction coefficient,
s_{the} = the thermoelastic source,
d_1 = the intrinsic heat dissipation, and
r = the external volume heat supply.

For the DP600 steel, $\rho = 7800\, kg/m^3$ and $C = 460\, J/kg/^{\circ}C$.

FIG. 4 Successive fatigue loadings (each block consists of 10^7 cycles).

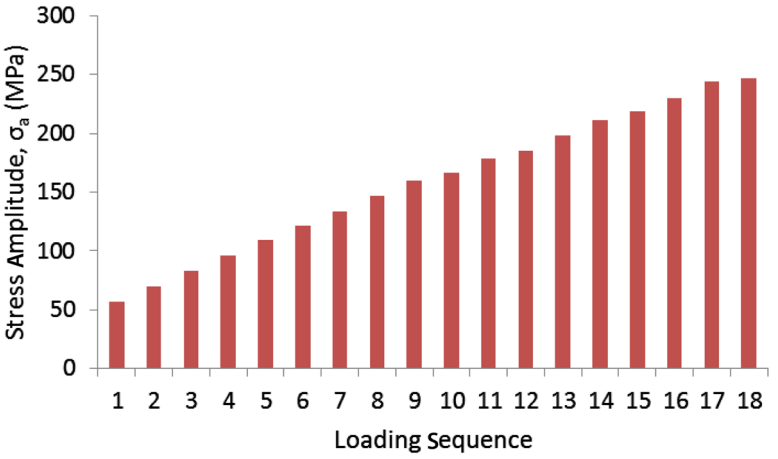

It is assumed that the volume heat source is time independent so it is expressed in Eq 2 as:

$$r = -kT_0 \tag{2}$$

in which T_0 is the initial equilibrium temperature. By assuming the material parameters ρ, C, and k to be constant and by introducing the temperature increase $\theta = T - T_0$, the heat diffusion equation (Eq 3) can be rewritten as:

$$\rho C\dot{\theta} - k\Delta\theta = s_{the} + d_1 \tag{3}$$

where Δ is the Laplace operator.

As suggested by Boulanger et al. [7], for symmetric boundary conditions and initial conditions corresponding to an uniform temperature field, it can be assumed that heat losses are linear with respect to the temperature variation. Therefore, it can be assumed that $-k\Delta\theta = \rho C\frac{\theta}{\tau}$, where τ is a time constant describing the thermal exchanges between the specimen and its environment. The heat diffusion equation is therefore rewritten as:

$$\rho C\dot{\theta} + \rho C\frac{\theta}{\tau} = s_{the} + d_1. \tag{4}$$

The thermal boundary conditions are not symmetrical in the present case because one end of the specimen is fixed to the horn and the other end is free, as discussed in Blanche et al. [12]. However, the thermographic images show that the specimen temperature field is symmetrical, as will be presented in the following section. That is why Eq 4 is considered here.

The time constant τ can be determined at the end of the test, just after the unloading when there is no applied stress; at that moment, the thermoelastic and intrinsic dissipation heat sources are zero, while the temperature increase is not null ($\theta \neq 0$). Therefore, the heat equation is reduced to:

$$\rho C\dot{\theta} + \rho C\frac{\theta}{\tau} = 0. \tag{5}$$

Solving Eq 5, the theoretical relation for temperature increase is obtained as:

$$\theta(t) = \theta_f \exp\left(\frac{-t}{\tau}\right) \tag{6}$$

where θ_f is the temperature increase measured when the loading stops. Thus, τ is estimated by fitting the experimental data with the theoretical evolution of θ.

Moreover because the loading frequency is high, due to the temporal inertia, it is not possible to measure the instantaneous value of θ but only its average value per cycle determined over numerous loading cycles, therefore, by denoting:

$$\tilde{u} = \frac{1}{nT_1}\int_t^{t+nT_1} u dt = \frac{f}{n}\int_t^{t+T_1} u dt \tag{7}$$

where T_1 is the period of the loading, f is the loading frequency, and n a number of cycles (Eq 7). The heat diffusion equation after the integration explained earlier is re-written in Eq 8 as:

$$\rho C\dot{\tilde{\theta}} + \rho C\frac{\tilde{\theta}}{\tau} = \tilde{s}_{the} + \tilde{d}_1. \tag{8}$$

As stated by Boulanger et al. [7], the sum of the thermoelastic power over one loading cycle is null ($\tilde{s}_{the} = 0$); thus, the final form of the heat diffusion equation is obtained in Eq 9:

$$\rho C\dot{\tilde{\theta}} + \rho C\frac{\tilde{\theta}}{\tau} = \tilde{d}_1. \tag{9}$$

Therefore, in the stabilized regime, when $\dot{\tilde{\theta}} = 0$, the average dissipation per cycle is easily determined from Eq 10 as:

$$\rho C\frac{\tilde{\theta}}{\tau} = \tilde{d}_1. \tag{10}$$

The mean dissipated energy per cycle can be obtained as $\tilde{d}_1/f$, where f is the loading frequency.

Results

Fig. 5 shows the evolution of the temperature for some of the loading steps. This figure shows that, for each loading step, the temperature increases suddenly in the

FIG. 5 Evolution of the mean temperature during several series of ultrasonic cyclic loadings.

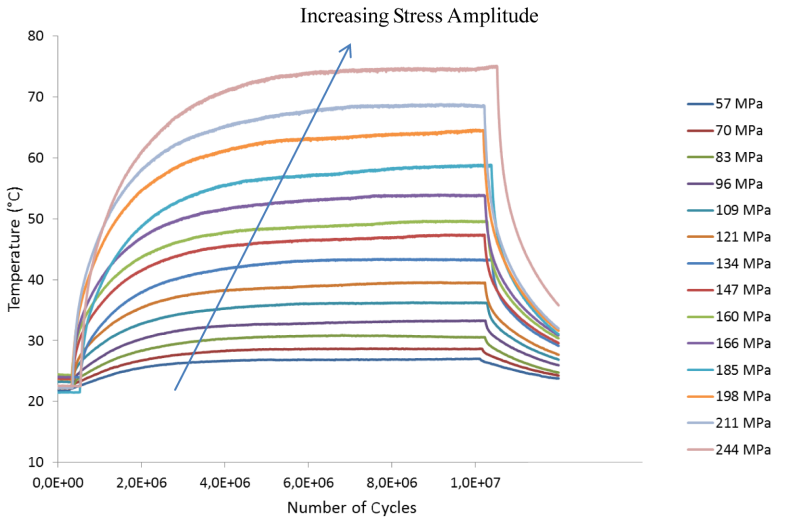

early stages of loading (after around 10^6 cycles) and then gradually reaches a steady state. In fact, the stabilization of the temperature corresponds to a balance between the mechanical energy dissipated into heat and the energy lost by convection and radiation at the specimen surface and by conduction inside the specimen. The higher the stress amplitude, the higher is the rate of temperature increase. The mean steady-state temperature elevation for each loading step defined as $\theta_f = T_{steady} - T_{initial}$ is plotted versus stress amplitude in Fig. 6. From this figure, it is clear that, by increasing the stress amplitude, the temperature elevation increases; for stress amplitudes lower than 60 MPa, the temperature increase remains lower than 10 °C. However, it reaches around 70 °C for higher stress amplitudes. As an instance, the specimen steady-state temperature field obtained from IR thermography is depicted in Fig. 7 for the stress amplitude of 102 Mpa. This figure shows that the temperature distribution is symmetrical.

Fig. 8 shows the values of the time constant τ obtained by matching Eq 6 and the evolution curve of temperature with time after the stop of the fatigue test for the various stress amplitudes displayed in Fig. 5. By increasing the stress amplitude up to 127 MPa, τ decreases from 20.5 s to 8 s; however, after this point, it reaches a plateau and remains approximately constant by increasing the stress. Taking into account the value of τ for the different stress amplitudes, the mean dissipated energy per cycle is calculated from the steady-state temperature. Fig. 9 depicts the change in dissipated energy per cycle as a function of stress amplitude. From this figure, it is clear that the higher the stress amplitude, the higher is the dissipated energy. Moreover, the dissipated energy per cycle is a quadratic function of stress amplitude.

FIG. 6 Temperature increase versus stress amplitude for DP600 steel under ultrasonic fatigue loading.

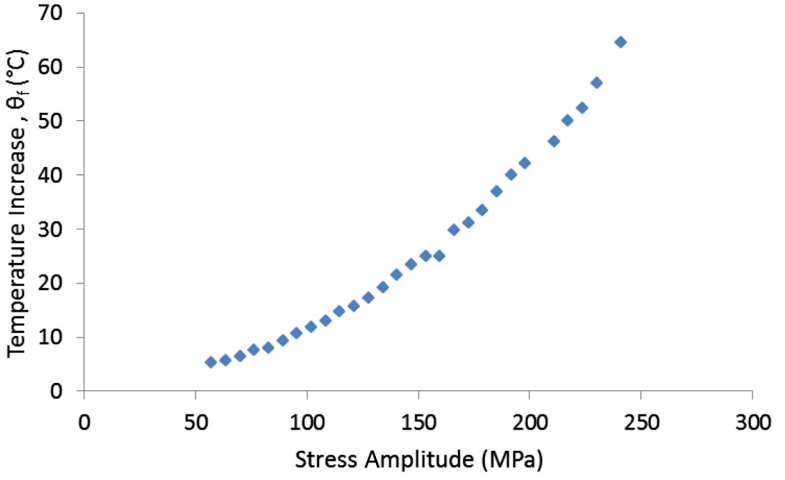

FIG. 7 Temperature field on the specimen surface for $\sigma_a = 102$ Mpa at $N = 8 \times 10^6$ cycles.

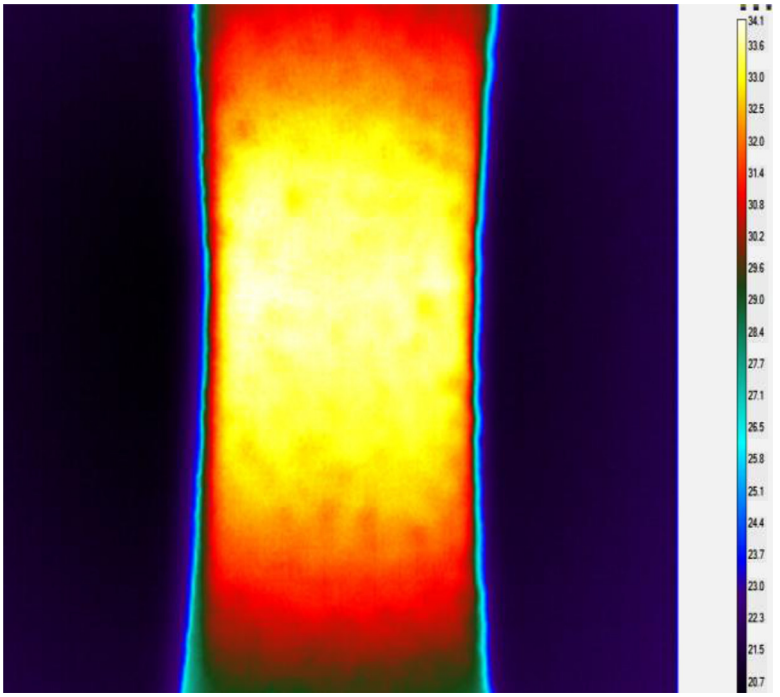

FIG. 8 The time constant, τ, versus stress amplitude.

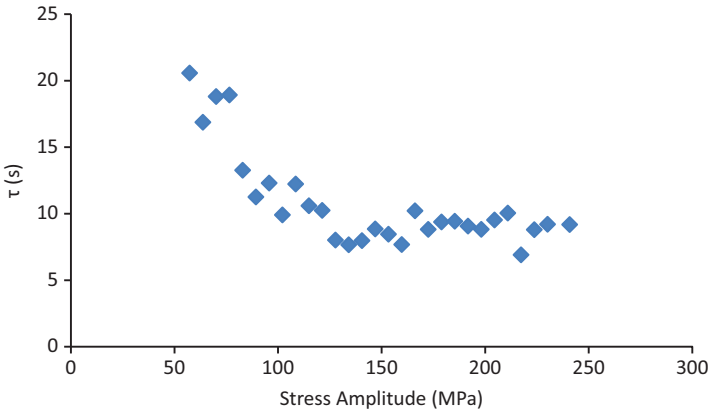

FIG. 9 Mean dissipated energy per cycle versus stress amplitude for the DP600 steel under ultrasonic loading.

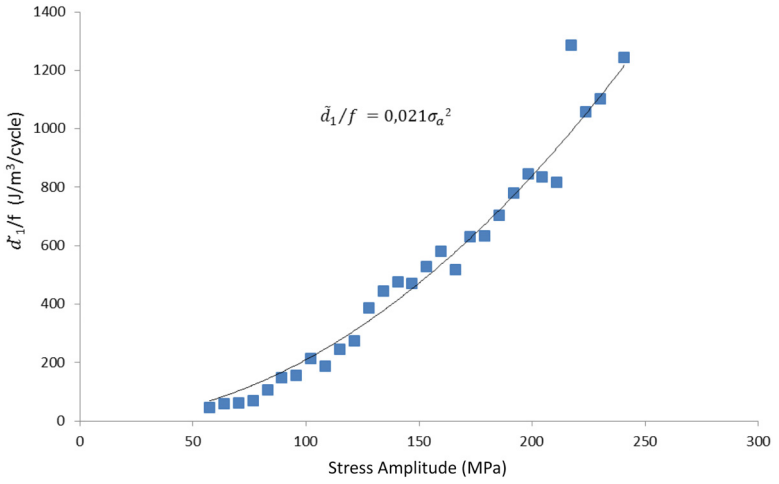

Discussion

For low stress amplitudes, below 250 MPa, the change in self-heating and dissipated energy per cycle with increasing temperature displays a quadratic form; therefore, a gradual increase in the slope of the curve is observed. Considering that the dissipated energy is due to an anelastic or inelastic material behavior characterized by constant properties leads to the following expressions for the dissipated energy [16]; assuming a prescribed sinusoidal stress with the amplitude σ_a and a Kelvin-Voigt model (spring and dashpot in parallel), the dissipated energy per cycle is written as [16]:

$$\frac{\tilde{d}_1}{f} = \frac{1}{f}\frac{2\eta(\pi\sigma_a)^2}{\frac{\mu^2}{f^2} + 4\pi^2\eta^2} \tag{11}$$

where μ and η are the elastic and viscous moduli, respectively.

In the case of a pure inelastic behavior and a zero mean stress, the dissipated energy per cycle is written as [16]:

$$\frac{\tilde{d}_1}{f} = \frac{1}{f}\frac{{\sigma_a}^2}{2\eta}. \tag{12}$$

In both cases, in the case of constant material properties (μ and η), the dissipated energy per cycle is a quadratic function of the stress amplitude. In this work, as the

dissipated energy per cycle is found to be a quadratic function of the stress amplitude for low stress amplitudes, it can be assumed that the material internal state remains nearly the same during cyclic loading. Because the hardness of the martensite is much higher than ferrite, dislocations are assumed to move only in the ferritic phase, which has a body-centered cubic (bcc) structure. In bcc metals, the flow stress strongly depends on temperature and strain rate at low temperatures. Mughrabi, Herz, and Stark [17] describe the temperature-dependent deformation of bcc metals by introducing two deformation modes based on a transition temperature, T_0. In the low-temperature (or thermally activated) mode ($T < T_0$), the screw dislocations are immobile and the edge dislocations move to and fro in a non-hardening quasi-recoverable manner. On the other hand, in the athermal mode ($T > T_0$), mobilities of the screw and edge dislocations are comparable, and screw dislocations can cross slip easily. In this mode, strain localization can occur on slip bands, and more energy can be dissipated because of high dislocation mobilities. The transition temperature, T_0, largely depends on strain rate and can be shifted to higher values at high strain rates. For instance, according to the flow behavior diagram reported by Campbell and Ferguson [18] for a 12 wt % carbon mild steel, T_0 would shift from 25 °C to 100 °C by increasing the strain rate from 0.01 s^{-1} to 1 s^{-1}. For ultrasonic fatigue loadings at low stress amplitudes from 60 to 247 MPa, the maximum strain rate ranges from 34 s^{-1} to 141 s^{-1}. Therefore, for such high strain rates, the transition temperature for the DP600 should be higher than room temperature. As a result, and as suggested by Favier et al. [14] for alpha-iron, the thermally activated mode, which is typical of a bcc structure, prevails at room temperature for a 20-kHz cyclic loading at low stress amplitudes. Therefore, the dissipated energy probably results from the to-and-fro motion of dislocations that result in slight changes in the material internal state and are consistent with Eqs 11 and 12.

In addition, the estimated values for dissipated energy per cycle are in agreement with results reported in the literature for alpha-iron. For instance, for the stress amplitude of 200 MPa, which is equal to 30 % of the ultimate stress amplitude, the dissipated energy per cycle is 800 J/m^3/cycle. This is consistent with the results obtained by Favier et al. for alpha-iron [14].

Conclusions

In this work, ultrasonic fatigue tests along with in situ IR thermography are conducted on flat specimens of DP600 steel. The self-heating diagrams are developed under ultrasonic loading for low stress amplitudes, and the dissipated energy per cycle is also determined. It is observed that, at low stress amplitudes, the dissipated energy per cycle is a quadratic function of the stress amplitude. The to-and-fro glide of the edge dislocations is considered to be the main dissipative mechanism. This motion is quasi-recoverable and leaves a quasi-constant dislocation structure (no cyclic hardening).

References

[1] Bathias, C., "There Is No Infinite Fatigue Life in Metallic Materials," *Fatigue Fract. Eng. Mater. Struct.*, Vol. 22, No. 7, 1999, pp. 559–565.

[2] Wu, T. and Bathias, C., "Application of Fracture Mechanics Concept to Ultrasonic Fatigue," *Eng. Fract. Mech.*, Vol. 47, No. 5, 1994, pp. 683–690.

[3] Stanzl-Tschegg, S. E., Mayer, H. R., and Tschegg, E. K., "High Frequency Method for Torsion Fatigue Testing," *Ultrasonics*, Vol. 31, No. 4, 1993, pp. 275–280.

[4] Wang, Q. Y., Berard, J. Y., Dubarre, A., Baudry, G., Rathery, S., and Bathias, C., "Gigacycle Fatigue of Ferrous Alloys," *Fatigue Fract. Eng. M.*, Vol. 22, No. 8, 1999, pp. 667–672.

[5] Furuya, Y., Matsuoka, S., Abe, T., and Yamaguchi, K., "Gigacycle Fatigue Properties for High-Strength Low-Alloy Steel at 100 Hz, 600 Hz, and 20 kHz," *Scripta Mater.*, Vol. 46, No. 2, 2002, pp. 157–162.

[6] Marines, I., Dominguez, G., Baudry, G., Vittori, J. F., Rathery, S., and Doucet, J. P., "Ultrasonic Fatigue Tests on Bearing Steel AISI-SAE 52100 at Frequency of 20 and 30 kHz," *Int. J. Fatigue*, Vol. 25, No. 9, 2003, pp. 1037–1046.

[7] Boulanger, T., Chrysochoos, A., Mabruand, C., and Galtier, A., "Calorimetric Analysis of Dissipative and Thermoelastic Effects Associated with the Fatigue Behavior of Steels," *Int. J. Fatigue*, Vol. 26, No. 3, 2004, pp. 221–229.

[8] Munier, R., Doudard, C., Calloch, S., and Weberb, B., "Towards a Faster Determination of High Cycle Fatigue Properties Taking into Account the Influence of a Plastic Pre-Strain from Self-Heating Measurements," *Procedia Eng.*, Vol. 2, No. 1, 2010, pp. 1741–1750.

[9] Doudard, C., Calloch, S., Hild, F., and Roux, S., "Identification of Heat Source Fields from Infrared Thermography: Determination of 'Self-Heating' in a Dual-Phase Steel by Using a Dog Bone Sample," *Mech. Mater.*, Vol. 42, No. 1, 2010, pp. 55–62.

[10] Doudard, C. and Calloch, S., "Influence of Hardening Type on Self-Heating of Metallic Materials under Cyclic Loadings at Low Amplitude," *Eur. J. Mech. A-Solids*, Vol. 28, No. 2, 2009, pp. 233–240.

[11] Doudard, C., Calloch, S., Hild, F., Cugy, P., and Galtier, A., "Identification of the Scatter in High Cycle Fatigue from Temperature Measurements," *C. R. Mecanique*, Vol. 332, No. 10, 2004, pp. 795–801.

[12] Blanche, A., Chrysochoos, A., Ranc, N., and Favier, V., "Dissipation Assessments during Dynamic Very High Cycle Fatigue Tests," *Exp. Mech.*, Vol. 55, No. 4, 2015, pp. 699–709.

[13] Ranc, N., Blanche, A., Ryckelynck, D., and Chrysochoos, A., "POD Preprocessing of IR Thermal Data to Assess Heat Source Distributions," *Exp. Mech.*, Vol. 55, No. 4, 2015, pp. 725–739.

[14] Favier, V., Blanche, A., Wang, C., Phung, N. L., Ranc, N., Wagner, D., Bathias, C., Chrysochoos, A., and Mughrabi, H., "Very High Cycle Fatigue for Single Phase Ductile Materials: Comparison between α-Iron, Copper, and α-Brass Polycrystals," *Int. J. Fatigue*, Vol. 93, No. 2, 2016, pp. 326–338.

[15] Munier, R., Doudard, C., Calloch, S., and Weber, B., "Determination of High Cycle Fatigue Properties of a Wide Range of Steel Sheet Grades from Self-Heating Measurements," *Int. J. Fatigue*, Vol. 63, 2014, pp. 46–61.

[16] Mareau, C., Favier, V., Weber, B., and Galtier, A., "Influence of the Free Surface and the Mean Stress on the Heat Dissipation in Steels under Cyclic Loading," *Int. J. Fatigue*, Vol. 31, Nos. 8–9, 2009, pp. 1407–1412.

[17] Mughrabi, H., Herz, K., and Stark, X., "Cyclic Deformation and Fatigue Behavior of α-Iron Mono- and Polycrystals," *Int. J. Fract*. Vol. 17, No. 2, 1981, pp. 193–220.

[18] Campbell, J. D. and Ferguson, W. G., "The Temperature and Strain-Rate Dependence of the Shear Strength of Mild Steel," *Philos. Mag*., Vol. 21, No. 169, 1970, pp. 63–82.